Proceedings of the ASME/BATH 2013 Symposium on Fluid Power & Motion Control
FPMC2013
October 6-9, 2013, Sarasota, Florida, USA

FPMC2013-4428

EFFICIENCY MODELING AND EXPERIMENTAL VALIDATION OF A VARIABLE DISPLACEMENT LINKAGE PUMP

Shawn Wilhelm, PhD Candidate
University of Minnesota
Minneapolis, MN, USA

Prof James Van de Ven
University of Minnesota
Minneapolis, MN, USA

ABSTRACT

The power density of hydraulic drive trains make variable displacement machines appealing to a wide range of applications such as mobile hybrid systems, displacement controlled actuation of heavy machinery, and hydrostatic transmissions for wind power. Current state of the art variable displacement pumps suffer from poor efficiencies at low displacements, thus limiting the potential benefits of hydraulic solutions. Here, a variable displacement linkage pump is presented as a promising method for achieving high efficiency across the full displacement range. In this paper, the linkage kinematics and dynamics are discussed, an energy loss model is presented and used to drive design decisions of a first generation prototype, and experimental results are presented to validate the model. It will be shown that this linkage-based, variable, positive displacement architecture shows promise as a highly efficient alternative to other axial piston machines across a wide range of displacements.

INTRODUCTION

There are many applications that can benefit from efficient variable displacement hydraulic pumps and motors, including hydraulic hybrid vehicles, hydrostatic wind turbine transmissions, agricultural equipment, and heavy machinery. Current variable displacement architectures suffer from poor efficiency when operating at low displacement conditions. This causes poor overall efficiencies in fluid power systems and prevents the use of hydraulics in other applications which could otherwise benefit from the intrinsic high power density of hydraulics. Several examples are now presented.

A hydrostatic transmission using a variable hydraulic pump could replace the mechanical transmission in the nacelle of a wind turbine and allow an AC generator to be run at constant speed by a fixed or variable hydraulic motor on the ground. Doing so would increase the power capabilities of the turbine, reduce the nacelle weight, and eliminate the need for expensive power electronics [1]. Large variations in wind speed require a pump/motor which could achieve high flow rates and also be efficient at normal wind conditions. Because a constant blade tip speed is preferred large, displacement variations are required.

In hydraulic hybrid vehicles, the displacement of the tractive pump/motor is directly related to the wheel torque and system pressure resulting in a wide range of operating conditions including low displacements and low pressures. A hydraulic hybrid four door passenger vehicle with an average pump/motor efficiency of 80% could achieve 80 mpg [2]. Other work has determined that low pump/motor efficiency at low displacement limits the capabilities of hydraulic hybrid off-road vehicles as well [3].

Heavy machinery employing displacement control with currently available variable pump/motors have shown a 50% energy savings over throttling valve control [4]. Further savings could be realized if these pump/motors had higher average efficiencies.

There are several types of positive displacement hydraulic pumps and motors including gear, screw, lobe, and piston machines. Of these machines, there are 3 main architectures commonly used in variable displacement applications: axial piston, bent axis, and vane. Much work has been done on improving the efficiency of these variable machines [5-7]. For the most part, these efforts have resulted in an increase in the maximum efficiency, but they have not significantly improved the low efficiency at low volumetric displacement. It is therefore reasonable to consider other methods of varying displacement.

An alternative approach is the use of pulse-width modulation to control the duty ratio of a fixed displacement pump using high speed on/off valves. Several works in this area show promise, but they have been hindered by losses associated with the limitations of valve switching speeds [8-10]. Another similar technique is digital control of the piston valves to turn individual cylinders on or off. Studies have shown that this method is promising for high efficiency at low displacement [11-13].

The crank-slider reciprocating piston pump/motor is an architecture which is not actively used for variable displacement. These pumps use pin joints, which require less lubrication and suffer smaller friction losses in comparison with hydrostatic bearings used in other variable displacement architectures. Other works and patents have presented the use of adjustable linkage for stroke variation of internal combustion engines [14-20], but little can be found with regards to a linkage-based variable hydraulic pump.

An introduction and synthesis method for designing a linkage for this application was previously introduced by the authors [21], and this paper expands upon the concept with a

prototype and experimental data. In the first section of this paper, the linkage overview and kinematic model are presented. The second section includes an energy loss model. In the third section, the prototype pump and experimental setup are shown. In the fourth section, experimental results are presented and compared to the model. The fifth section presents a discussion of the results, and the final section contains the concluding remarks.

NOMENCLATURE

A_p	$Piston\ cross\ sectional\ area\ [m^2]$
A_s	$Acceleration\ of\ slider\ link\ \left[\frac{m}{s^2}\right]$
$\boldsymbol{Ag}_i$	$Acceleration\ vector\ of\ CG\ of\ link\ i\ \left[\frac{m}{s^2}\right]$
d_p	$Piston\ diameter\ [m]$
E_{cf}	$Energy\ of\ coulomb\ friction\ [J]$
E_{ql}	$Energy\ of\ leakage\ flow\ [J]$
E_v	$Energy\ of\ viscous\ friction\ [J]$
F_{cf}	$Force\ of\ coulomb\ friction\ [J]$
$\boldsymbol{F}_{ij}$	$Force\ vector\ of\ load\ applied\ by\ j\ on\ i\ [N]$
F_N	$Normal\ force\ applied\ to\ pin\ \ [N]$
F_p	$Force\ applied\ to\ piston\ \ [N]$
F_v	$Viscous\ friction\ force\ [N]$
h	$Piston\ cylinder\ gap\ height\ [m]$
l_i	$Scalar\ length\ of\ ith\ link\ [m]$
l_p	$Piston\ length\ [m]$
$\boldsymbol{P}$	$Vector\ (complex\ number)\ \ location\ of\ adjustment\ pivot\ [m]$
p_x	$Distance\ to\ axis\ of\ slide\ from\ x-axis\ [m]$
Q_{leak}	$Leakage\ flow\ rate\ \left[\frac{m^3}{s}\right]$
Q_{out}	$Flowrate\ from\ pump\ \left[\frac{m^3}{s}\right]$
r	$Radius\ of\ pin\ [m]$
R_{ij}	$Radius\ from\ pin\ i\ to\ CG\ of\ link\ j\ [m]$
T_{12}	$Linkage\ input\ torque\ [Nm]$
v_s	$Piston\ velocity\ \left[\frac{m}{s}\right]$
W_{in}	$Shaft\ Work\ [J]$
$W_{in_{ideal}}$	$Ideal\ input\ work\ [J]$
W_{out}	$Pumping\ Work\ [J]$
γ_{min}	$Minimum\ transmission\ angle\ [rad]$
η_{pump}	$Efficiency\ of\ pump\ [unitless]$
μ_d	$Dynamic\ viscosity\ of\ working\ fluid\ [Pa\ s]$
μ_k	$Dynamic\ friction\ coefficient\ [unitless]$
ω_i	$Angular\ velocity\ of\ ith\ link\ \left[\frac{rad}{s}\right]$
θ_i	$Global\ angle\ of\ ith\ link\ [rad]$

LINKAGE OVERVIEW

A previous work describes the type synthesis, and possible configurations of a variable displacement slider linkage. The linkage studied in this paper is of the overlapped, R_{1max} configuration and is shown in Figure 1 [21]. It consists of a base four bar crank-rocker mechanism which includes the input crank, coupler link, and rocker link. The position of the ground pivot of the rocker link can be adjusted through the dashed arc centered at the adjustment point ***P***. The connecting rod joins the sliding link to the base four bar at the coupler point. When the adjustable ground pivot is collinear with the axis of slide, the sliding link will exhibit no translation when the crank is rotated. As the adjustable ground pivot moves away from the axis of slide, the slider link will translate.

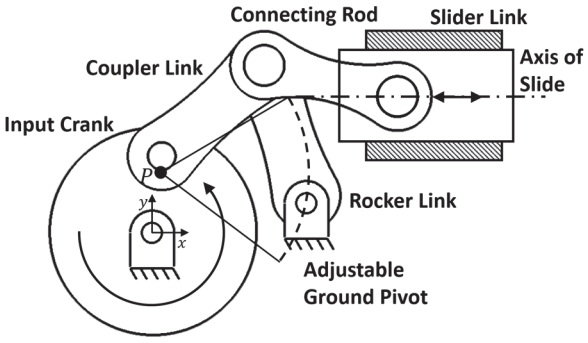

FIGURE 1. SCHEMATIC OF THE ADJUSTABLE LINKAGE

An additional benefit of this linkage is that the slider returns to the same top dead center position independent of displacement setting. This means that all of the working fluid, except for a small constant dead volume, can be ejected on every stroke to minimize compressibility losses.

Kinematic Equations of Motion

The linkage is described mathematically using complex number notation and rotation operators. Below the vector loop equations are presented with reference to Figure 2.

$$l_2 e^{i\theta_2} + l_3 e^{i\theta_3} - l_4 e^{i\theta_4} - l_1 e^{i\theta_1} = 0 \qquad 1$$

$$l_4 e^{i\theta_4} - l_5 e^{i\theta_5} - l_6 - l_7 1i = 0 \qquad 2$$

With the link lengths known and the input crank angle θ_2 given as an input, the four unknowns $\theta_3, \theta_4, \theta_5,$ and l_3 are solved for using the methods described by Norton [22]. Norton also describes the solution for the angular and linear velocities and accelerations for each link and joint respectively. For brevity, the equations of motion are included in Appendix A.

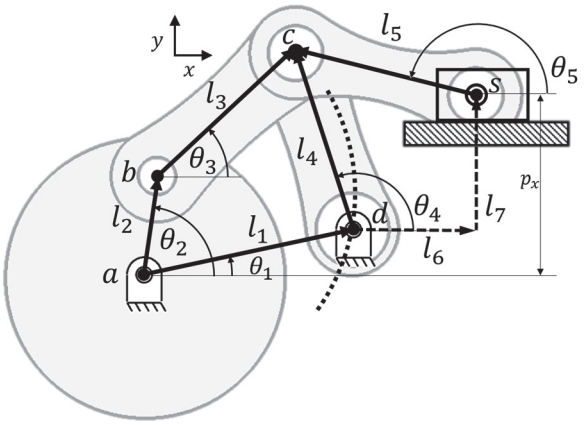

FIGURE 2. VECTOR LOOP DIAGRAM OF LINKAGE FOR POSITION ANALYSIS

The position analysis can be completed for any displacement where l_1 and θ_1 vary depending on the position of the adjustable ground pivot. To control the transmission angle, γ_{min}, between links 3 and 4, l_1 is limited between $l_{1_{max}}$ and $l_{1_{min}}$ which are defined as follows:

$$l_{1_{max}} = \sqrt{l_3^2 + l_4^2 - 2\cos(\pi - \gamma_{min})\, l_3 l_4} \; - l_2 \qquad 3$$

$$l_{1_{min}} = \sqrt{l_3^2 + l_4^2 - 2\cos\gamma_{min} l_3 l_4} \; + l_2 \qquad 4$$

The adjustment point $\boldsymbol{P}$ is described as:

$$l_p = l_3 - l_2 \qquad 5$$

$$\theta_p = \cos^{-1}\left[\frac{l_{1_{max}}^2 + l_p^2 - l_4^2}{2 l_{1_{max}}^2 l_p^2}\right] \qquad 6$$

$$\boldsymbol{P} = l_p e^{1i\theta_p} \qquad 7$$

Internal Forces and Torques

Once the position, velocity, and acceleration components of the linkage are solved, a dynamic analysis of the pin forces and input torque is completed. For this analysis, friction is considered negligible relative to the piston force and bearing loads. Later, friction energy is calculated from these results when evaluating work input. Force balance equations of the linkage are solved at different angular steps of the input crank angle θ_2. Links 3-5 each provide three equations, the slider produces two additional equations, and the input link one final equation to resolve the dynamic force and moment balance. In total, there are twelve equations and twelve unknowns: the ten pin forces, the slider reaction force, and the input torque.

Figure 3 shows the physical system with labeled forces and locations of the center of mass of each link. Since the slider has no angular velocity, there is no moment to balance, and solving for the location of the center of mass is unnecessary. Additionally, the input crank is considered balanced about its rotational axis. The system of equations for the force analysis are included in Appendix B.

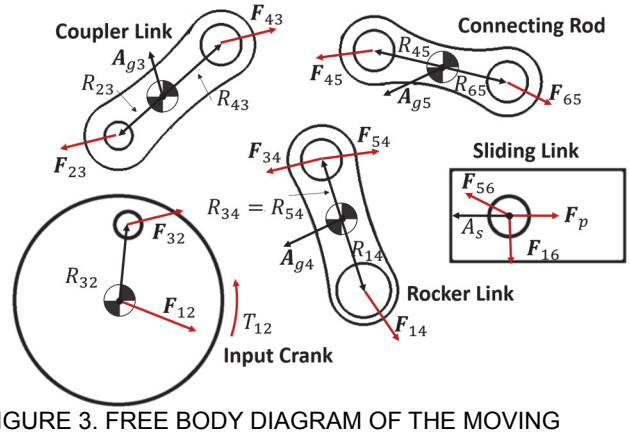

FIGURE 3. FREE BODY DIAGRAM OF THE MOVING COMPONENTS OF THE LINKAGE SHOWING FORCES AND CENTERS OF MASS

ENERGY MODELING

With the kinematics and dynamics of the linkage resolved, the pumping work and energy losses of the system can be modeled. Three sources of losses are considered: viscous friction between the piston and cylinder, coulomb friction of the linkage pins and crosshead bearing, and leakage across the piston cylinder gap.

Numerical Modeling

The kinematic and dynamic equations are solved at multiple steps of the input crank angle, θ_2, for a complete revolution. The output values of these equations are then used as inputs to solve the energy loss model at each input crank angle, which is then integrated over a complete revolution to determine the total energy loss per cycle.

Assumptions

Valve losses are considered outside the scope of this design and are not considered here. Because of the small dead volume of 2 cm^3, compressibility losses only account for 0.14% of total losses and are also excluded.

This model assumes that there is no piston rotation or eccentricity relative to the cylinder, and, as a result, the clearance gap is constant. This assumption is valid with a linkage pump because the design allows for a crosshead bearing and such a bearing design reacts the piston side loads unlike axial-piston pumps where the pistons react these loads.

Viscous Friction Energy Losses

Viscous friction is caused by the shearing of the working fluid in the gap between the piston and the cylinder due to their

relative motion. From Newton's law of viscosity, the viscous friction force in a piston clearance seal can be expressed as:

$$F_v = \pi d_p l_p \frac{\mu_d}{h} v_s \quad (8)$$

where d_p is the piston diameter, l_p is the piston length, μ_d is the dynamic viscosity of the fluid, h is the radial piston clearance, and v_s is the relative velocity of the piston and cylinder which is obtained from equation A-20.

Here the flow is considered fully developed with a no slip condition at the piston and cylinder walls. The fluid is considered incompressible and Newtonian with a uniform viscosity. The energy loss due to viscous friction is determined by integrating the viscous friction force over a complete cycle as expressed by:

$$E_v = \int F_v dx = \int F_v v_s dt \quad (9)$$

Coulomb Friction Energy Losses

The pin joints are modeled as simple bearings using coulomb friction as depicted in Figure 4. The frictional energy loss over a cycle is found by integrating the friction force with respect to the angle of rotation between the pin and the link:

$$F_{cf} = \mu_k F_N \quad (10)$$

$$E_{cf} = r\int F_{cf} d\theta = r\int F_{cf} \omega dt \quad (11)$$

where F_{cf} is the resultant friction force which opposes the direction of motion at the outer surface of the pin, F_N is the magnitude of the force applied to the joint, r is the radius of the pin, $d\theta$ is the relative change in angle between the link joint and the pin, and ω is the relative angular velocity between the link joint and the pin.

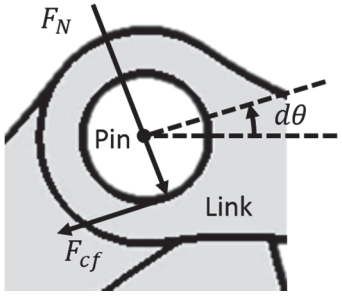

FIGURE 4 COULOMB FRICTION DIAGRAM SHOWING PIN JOINTS RELATIVE TO VARIOUS LINKS

These equations are used to calculate the friction energy at each of the pin joints, which are then be summed to calculate the total energy lost to pin friction.

In addition to the coulomb friction in the pin joints, there is additional friction loss at the crosshead bearing, described by:

$$F_{cf_{crosshead}} = -\mu_{k_c} F_{16y} \quad (12)$$

$$E_{cf_{crosshead}} = \int F_{cf} v_s dt \quad (13)$$

Clearance Seal Energy Losses

The pressure drop across the piston and the relative motion between the piston and the cylinder creates a leakage flow. As described by Ivantysn and Ivantysnova, the leakage flow rate for a piston clearance seal is [23]:

$$Q_{leak} = \frac{\pi d_p \left(6\mu_d l_p h v_s - \Delta P h^3\right)}{12\mu_d l_p} \quad (14)$$

where ΔP is the differential pressure across the piston at a given time step. Here the flow rate is derived from Couette–Poiseulle equation assuming laminar flow and the piston cylinder gap is simulated as the gap between parallel plates.

Positive leakage flow rate is considered unrecoverable flow passed the piston. The energy loss associated with this leakage is calculated by integrating the leakage flow with respect to time over a complete cycle:

$$E_{ql} = \int \Delta P Q_{leak} dt \quad (15)$$

Input Work

With the system losses known, the input work of the pumping mechanism is calculated. The ideal input work is defined as:

$$W_{in_{ideal}} = \int \omega_2 T_{12} dt \quad (16)$$

where ω_2 and T_{12} are solved from the kinematic and dynamic analysis, but do not include the losses. The total work input is therefore the sum of the ideal input work and losses:

$$W_{in} = W_{in_{ideal}} + E_{vf} + E_{cf} + E_{ql} \quad (17)$$

Output Work

The energy output of the pump is defined as:

$$W_{out} = \int \Delta P Q_{out} dt \quad (18)$$

where Q_{out} is the output flow of the pump which can be evaluated as:

$$Q_{out} = A_p v_s \quad (19)$$

where A_p is the piston area. It can therefore be shown that:

$$W_{out} = \int F_p v_s dt \quad (20)$$

where F_p is the force applied to the piston.

Pumping Efficiency

With the work input and work output determined, efficiency is defined as:

$$\eta_{pump} = \frac{W_{out}}{W_{in}} \qquad 21$$

METHODS

To evaluate the model of the previous section, a low power prototype pumping unit was constructed and experiments were conducted. In this section, the prototype is introduced, the experimental setup is presented and the experimental method is described.

Prototype Pumping Machine

The links were designed to accommodate a pressure of 5 MPa with a maximum volumetric displacement of 8.7 cm^3/rev. The linkage kinematics drove the linkage sizing, and the energy model was used to size and tolerance the hydraulic components. For flow control, Vonberg inline check valves are used on the inlet and outlet ports. A hydraulic cylinder controls the displacement by actuating the displacement adjustment link, causing the adjustable ground pivot to rotate about the adjustment point, *P.* Figure 5 shows a cross sectional view of the mechanism. For brevity, the design process is not included here, but the design variables are listed in Table 1.

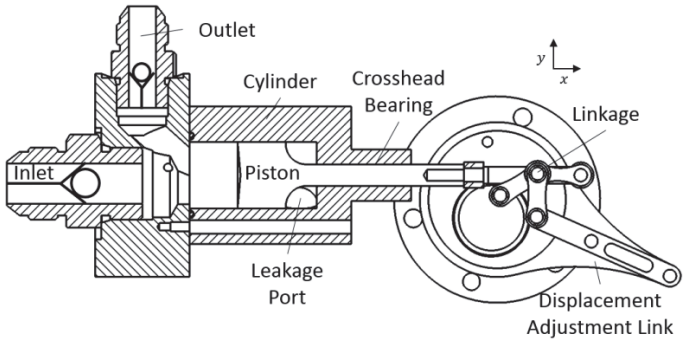

FIGURE 5 PROTOTYPE VARIABLE DISPLACEMENT LINKAGE PUMP USED FOR LOW POWER EXPERIMENTAL VALIDATION

Experimental Setup

A non-contact torque transducer and optical encoder were used to measure the torque and angular velocity of the input shaft and allow for the calculation of the input work. A pressure transducer was used to measure the pressure in the cylinder in order to evaluate the piston force, F_p. Additionally, a pressure transducer measured the system pressure, which is controlled by a pressure relief valve. A gear flow meter measured the system flow rate, allowing for the evaluation of work output. A hydraulic accumulator is included to maintain the set pressure and smooth flow pulsations. A schematic of the experimental setup is provided in Figure 6.

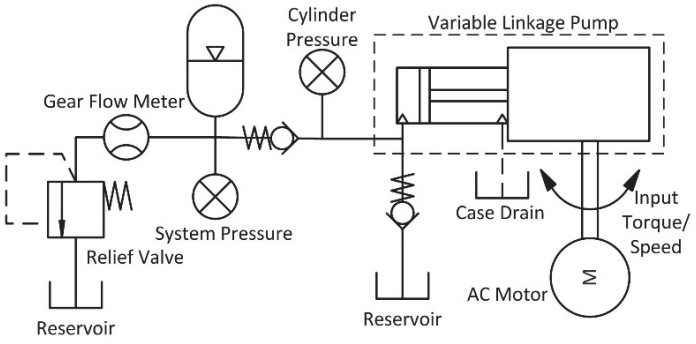

FIGURE 6 HYDRAULIC CIRCUIT DIAGRAM DISPLAYING THE EXPERIMENTAL SETUP

A hydraulic actuator controls the position of the adjustable ground pivot as previously described. The angular velocity of the AC motor and input shaft are controlled using a variable frequency drive. For certain experiments, a gear reducer with a ratio of 10:1 is used to prevent large angular velocity fluctuations at low shaft speeds.

TABLE 1 DESIGN TABLE OF PROTOTYPE VALUES FOR MODELING

PROTOTYPE DESIGN TABLE

Symbol	Description	Value	Unit
d_p	Piston Diameter	0.0246	$[m]$
h	Piston Cylinder Gap Height	4.00	$[\mu m]$
l_2	Length of Link 2	0.0089	$[m]$
l_3	Length of Link 3	0.016	$[m]$
l_4	Length of Link 4	0.016	$[m]$
l_5	Length of Link 5	0.016	$[m]$
l_p	Length of Piston Sealing Surface	0.0178	$[m]$
P	Location of Pivot Point	$.0021 + .0068i$	$[m]$
p_x	Distance to axis of slide from axis	0.0158	$[m]$
r	Pin radius	0.0024	$[m]$
μ_d	Coefficient of dynamic viscosity	0.065	$[Pa\ s]$
μ_k	Coefficient of friction for pins [24]	0.173	$[unitless]$
μ_{k_c}	Coefficient of friction for crosshead bearing [24]	0.12	$[unitless]$
γ_{min}	Minimum linkage transmission angle	0.5236	$[rad]$

Experimental Methods

A series of 6 experiments were conducted with the pressure varying between 1.2 MPa and 3.45 MPa at input speeds between 3 Hz and 9 Hz. Data were collected for a total of 5 seconds per

experiment at a frequency of 10 kHz. A digital low-pass filter with a pass band of 10 times the operating frequency was applied to the data to remove high frequency noise associated with the AC drive and other electronic devices in the lab.

Since the input crank returns to the same position at top dead center (TDC) independent of displacement, this point is used to align the data with the model in order to estimate v_s. To determine the TDC position of the piston, the cylinder pressure is analyzed to find the point in time at which the pressure begins to fall from system pressure to tank pressure, which is assumed to be the time at which the piston begins to retract.

The experimentally measured cylinder pressure and input crank angle are inserted into the model to predict the system work input and work output. These predicted values are then compared to the measured work input and work output for evaluating the model.

RESULTS

Figure 7 compares the experimentally measured work output to that predicted by the model for various pressures and frequencies. The model results are for the operating speed and pressure observed at different experimental data points. Figure 8 compares the model predicted and experimentally measured work input at various pressures and frequencies.

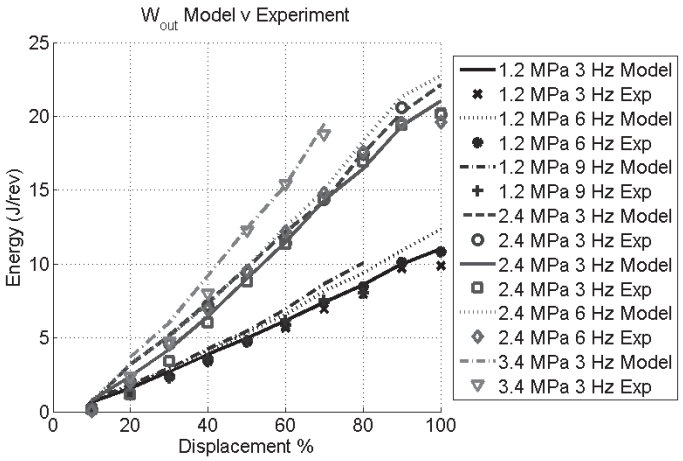

FIGURE 7 WORK OUTPUT EXPERIMENTAL DATA PLOTTED AGAINST MODEL AT VARIOUS FREQUENCIES AND PRESSURES

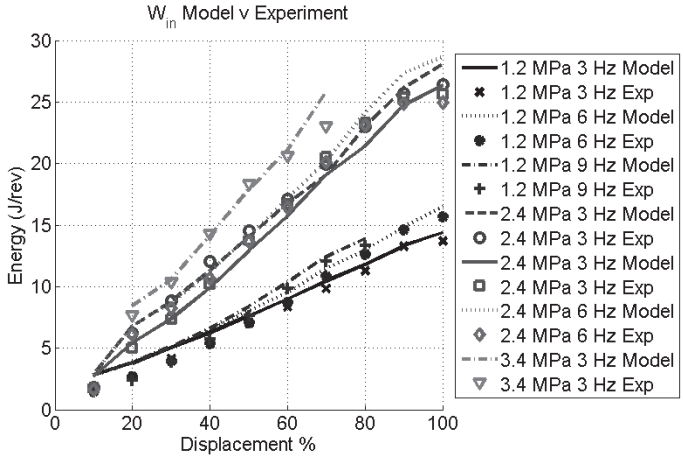

FIGURE 8 WORK INPUT EXPERIMENTAL DATA PLOTTED AGAINST MODEL AT VARIOUS FREQUENCIES AND PRESSURES

DISCUSSION

Figure 7 and Figure 8 show close agreement between the model and experiment results for both the work in and work out. The slight discrepancies at low displacement cases can be attributed to the small working volume. For example, at 10% of maximum displacement, a volume of 0.87 cm^3/rev of working fluid is ejected from the pumping cylinder. A significant portion of this displaced volume is thought to be lost to the displacement of the check valve poppet, and possibly the deflection in the linkage.

Additionally, at large displacements the model over-predicts pumping work output. The linkage experiences poor transmission angles and is loaded for the longest period at high displacement. Resultant deflection of the linkage leads to a reduction in piston displacement and subsequently reduction is work output.

Generally speaking, the work input model achieves closer agreement with the experiment than does the work output model. This is largely because the work input model relies on pressure data measured from the cylinder as well as the angle of the input shaft. The work output model does not consider valve losses, but the experimental data is measured downstream of the check valve. This is done to minimize the dead volume of the pumping cylinder, and because the design does not include active valves. Much of the losses associated with passive poppet style check valves can be alleviated in the future by using active valves.

With the model validated, it can be extrapolated to give more information on the efficiency of the presented linkage-based design. As seen in Figure 9, the largest energy loss term is coulomb friction. Here, the system is modeled at 2.4 MPa and 3 Hz to show a case which has been experimentally validated. Because both friction and work output scale almost linearly with velocity, the overall efficiency is largely unaffected by changes in pumping frequency. To demonstrate this point, a contour plot of the model efficiency is presented in Figure 10. Here the

pressure is held constant at 21 MPa and the frequency is varied between 1 and 60 Hz.

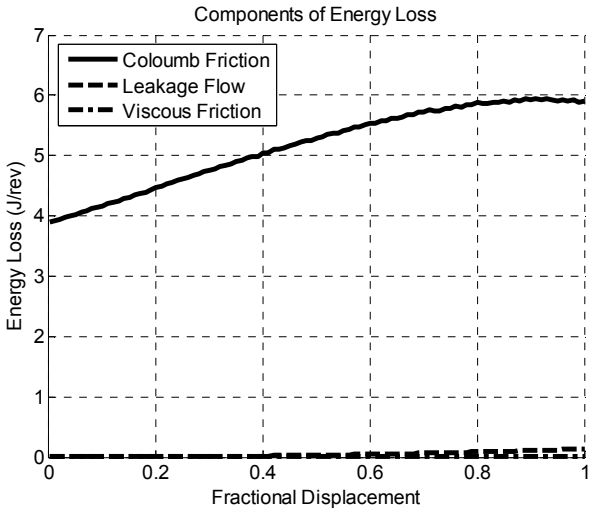

FIGURE 9 CONTRIBUTIONS OF VARIOUS LOSS TERMS AS A FUNCTION OF DISPLACEMENT AT 2.4MPa AND 3Hz OF PRESENT DESIGN

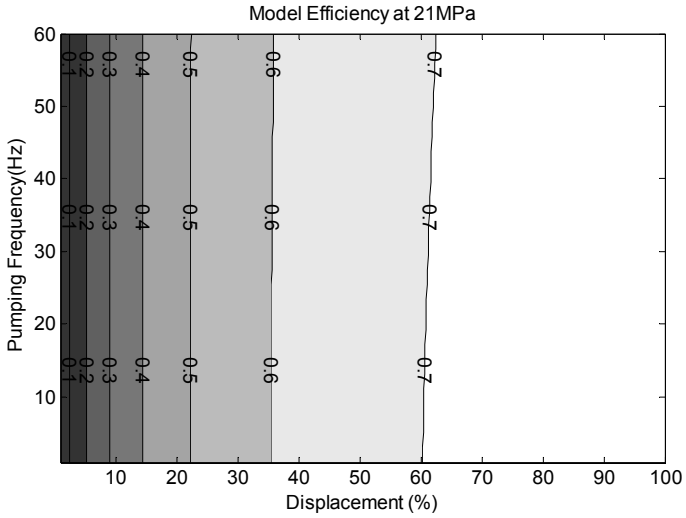

FIGURE 10 COUNTOUR PLOT OF MODEL EFFICIENCY AT CONSTANT PRESSURE AND VARYING SYSTEM FREQUENCIES OF PRESENT DESIGN

Similarly, Figure 11 shows a contour plot of the efficiency model with the pumping frequency at 30 Hz and the system pressure is varied between 1 and 35 MPa. Because coulomb friction scales linearly with applied normal force, which is a function of cylinder pressure, efficiency is generally unaffected by pressure. This rule does not hold at low pressure, where the losses are large relative to the work output.

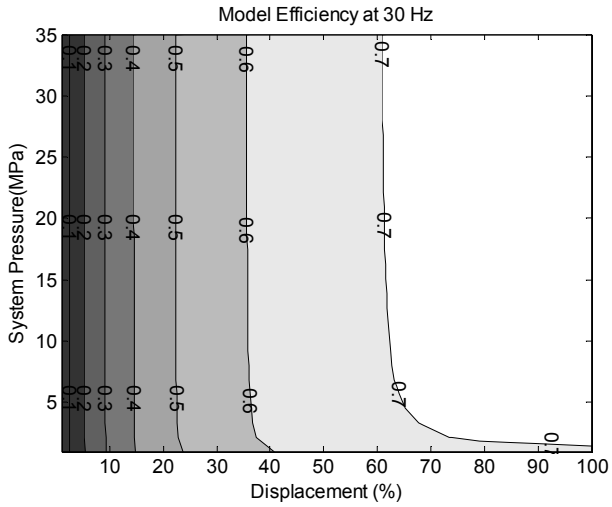

FIGURE 11 CONTOUR PLOT OF MODEL EFFICIENCY AT CONSTANT PUMPING FREQUENCY AND VARYING PRESSURES OF PRESENT DESIGN

When considering the concept of high efficiency at low displacement, the current design does not appear to be more efficient than some axial piston architectures. This, however, is due to the high friction plain bearings used in the pin joints. If lower friction rolling element bearings were used, which have an equivalent dynamic coefficient of friction of 0.005 [25], the efficiency values would be higher, as demonstrated in Figure 12. Here the pressure and frequency are held constant at 21 MPa and 30 Hz to evaluate the efficiency at various displacements.

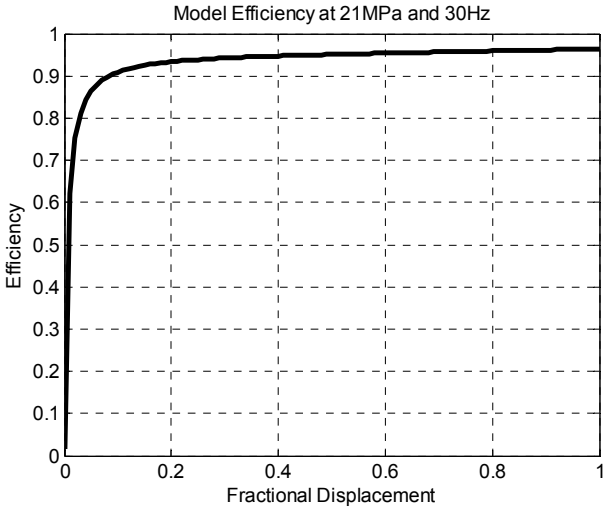

FIGURE 12 EFFICIENCY CURVE VS DISPLACEMENT FOR A PUMP WITH ROLLING ELEMENT BEARINGS AT 21 MPa AND 30 Hz

For these conditions, the efficiency values are greater than 90% for displacements above 10%. As previously demonstrated, the efficiency is largely independent of frequency and pressure, which shows that a linkage-based variable displacement pump

has the potential to be highly efficient at a wide range of operating conditions.

However, efficiency is not the only requirement of a hydraulic pump. Further work is needed to address the noise, vibrations, compactness, and flow ripple of a variable displacement linkage pump. The noise and vibration can be addressed with force and moment, as well as multi-cylinder, balancing of the linkage. Balancing was not considered here because the linkage experiences less than 50 N of shaking force at 30 Hz. Additionally, an inline cylinder arrangement can be used to minimize flow ripple. This single cylinder design prototype stands to demonstrate the viability of this new architecture.

CONCLUSSIONS

A model, prototype, and experimental data of a linkage-based variable displacement pumping machine have been presented. The experiments agree well with the model, which shows the efficiency of this architecture is largely unaffected by pressure and operating frequency. If low friction roller element bearings are used in the pin joints of the linkage, the linkage-based pump is expected to have efficiencies greater than 90% for displacements greater than 10% for the majority of operating conditions, not including valve related losses.

Further work is needed to evaluate and refine the design for other criteria such as compactness, noise, pressure ripple, and incorporation of active valves that would allow both pumping and motoring operation.

These results show promise for the linkage-based variable displacement pump as a viable solution to achieve high efficiency at low displacement which can further the potential of modern fluid power systems.

ACKNOWLEDGMENTS

This work is supported by the National Science Foundation under grant number EFRI-1038294.

REFERENCES

[1] S.H Salter, M. R., 1984, "Hydraulics for Wind," European Wind Energy ConferenceHamburg Germany, pp. 534-541.

[2] Van de Ven, J. D., Olson, M. W., and Li, P. Y., "Development of a hydro-mechanical hydraulic hybrid drive train with independent wheel torque control for an urban passenger vehicle," Proc. Proceedings of the National Conference on Fluid Power, Citeseer, p. 503.

[3] Comellas, M., Pijuan, J., Potau, X., Nogués, M., and Roca, J., 2013, "Efficiency sensitivity analysis of a hydrostatic transmission for an off-road multiple axle vehicle," International Journal of Automotive Technology, 14(1), pp. 151-161.

[4] Williamson, C., Zimmerman, J., and Ivantysynova, M., "Efficiency Study of an Excavator Hydraulic System Based on Displacement-Controlled Actuators," Proc. Bath/ASME Symposium on Fluid Power and Motion Control.

[5] Wieczorek, U., and Ivantysynova, M., 2002, "Computer aided optimization of bearing and sealing gaps in hydrostatic machines- the simulation tool CASPAR," International Journal of Fluid Power, 3(1), pp. 7-20.

[6] Manring, N. D., 2003, "Valve-plate design for an axial piston pump operating at low displacements," Journal of Mechanical Design, 125(1), pp. 200-205.

[7] Inaguma, Y., and Hibi, A., 2007, "Reduction of friction torque in vane pump by smoothing cam ring surface," Proceedings of the Institution of Mechanical Engineers, Part C: Journal of Mechanical Engineering Science, 221(5), pp. 527-534.

[8] Rannow, M., Tu, H., Li, P. Y., and Chase, T., "Software enabled variable displacement pumps-experimental studies," Proc. Proceedings of the 2006 ASME-IMECE.

[9] Tu, H., Rannow, M. B., Wang, M., Li, P. Y., and Chase, T. R., "Modeling and validation of a high speed rotary PWM on/off valve," Proc. Proceedings of the ASME Dynamic Systems and Control Conference 2009, pp. 12-14.

[10] Wang, M., Li, P. Y., Chase, T. R., and Van de Ven, J. D., 2012, "Design, Modeling, and Validation of a High-Speed Rotary Pulse-Width-Modulation On/Off Hydraulic Valve," Journal of dynamic systems, measurement, and control, 134, pp. 061002-061001.

[11] Ehsan, M., Rampen, W., and Salter, S., 2000, "Modeling of digital-displacement pump-motors and their application as hydraulic drives for nonuniform loads," Journal of dynamic systems, measurement, and control, 122(1), pp. 210-215.

[12] Linjama, M., "Digital fluid power–state of the art," Proc. Proceedings of the 12th Scandinavian international conference on fluid power, SICFP'11, pp. 331-353.

[13] Yigen, C., 2012, "Control of a Digital Displacement Pump," Department of Energy Technology, Aalborg University.

[14] Pierce, J., 1914, "Variable Stroke Mechanism,"United States of America.

[15] Pouliot, H. N., Delameter, W. R., and Robinson, C. W., 1977, "A Variable Displacment Spark-Ignition Engine," No. 770114, SAE International.

[16] Nelson, C. D., 1985, "Variable Stroke Engine,"United States of America.

[17] Yamin, J. A. A., and Dado, M. H., 2004, "Performance simulation of a four-stroke engine with variable stroke-length and compression ratio," Applied Energy, 77(4), pp. 447-463.

[18] Freudenstein, F., and Maki, E., "Development of an optimum variable-stroke internal-combustion engine mechanism from the viewpoint of kinematic structure," ASME.

[19] Freudenstein, F., and Maki, E., "Kinematic structure of mechanisms for fixed and variable-stroke axial-piston reciprocating machines," ASME.

[20] Freudenstein, F., and Maki, E. R., 1981, "Variable displacement piston engine," Google Patents.

[21] Wilhelm, S., and Van de Ven, J. D., 2011, "Synthesis of a Variable Displacement Linkage for a Hydraulic Transformer," International Design Engineering Technical Conferences & Computers and Information in Engineering Conference, ASME, Washington, DC, p. 8.

[22] Norton, R. L., 2008, Design of Machinery An Introduction to the Synthesis and Analysis of Mechanisms and Machines, McGraw-Hill, Boston.
[23] Ivantysyn, J., and Ivantysynova, M., 2001, "Hydrostatic pumps and motors," New Dehli: Academic Books International.
[24] Beardmore, R., 2013, "ROYMECH Friction Factors," http://www.roymech.co.uk/Useful_Tables/Tribology/co_of_frict.htm.
[25] Beardmore, R., 2010, "Roller Bearing Friction," http://www.roymech.co.uk/Useful_Tables/Tribology/Bearing%20Friction.html.

Appendix A: Kinematic equations of motion

With input crank angle, θ_2 as an input, the following set of equations determine the unknown base fourbar link angles θ_3 and θ_4.

$$K_1 = \frac{l_1}{l_2} \quad \text{A-1}$$

$$K_2 = \frac{l_1}{l_4} \quad \text{A-2}$$

$$K_3 = \frac{l_2^2 - l_3^2 + l_4^2 + l_1^2}{2l_2l_4} \quad \text{A-3}$$

$$K_4 = \frac{l_1}{l_3} \quad \text{A-4}$$

$$K_5 = \frac{l_4^2 - l_1^2 - l_2^2 - l_3^2}{2l_2l_3} \quad \text{A-5}$$

$$A = \cos\theta_2 \ - K_1 + K_2\cos\theta_2 \ + K_3 \quad \text{A-6}$$

$$B = -2\sin\theta_2 \quad \text{A-7}$$

$$C = K_1 - (K_2 + 1)\cos\theta_2 + K_3 \quad \text{A-8}$$

$$\mathrm{D} = \cos(\theta_2) - K_1 + K_4\cos\theta_2 \ + K_5 \quad \text{A-9}$$

$$E = -2sin\theta_2 \quad \text{A-10}$$

$$F = K_1 - (K_4 + 1)\cos\theta_2 + K_5 \quad \text{A-11}$$

$$\theta_3 = 2\tan^{-1}\frac{-E - \sqrt{E^2 - 4DF}}{2D} + \theta_1 \quad \text{A-12}$$

$$\theta_4 = 2\tan^{-1}\frac{-B - \sqrt{B^2 - 4AC}}{2A} + \theta_1 \quad \text{A-13}$$

With θ_4 known, the slider diad position can be evaluated.

$$l_7 = p_x - l_1\cos\theta_1 \quad \text{A-14}$$

$$\theta_5 = \sin^{-1}\left(\frac{l_4\sin\theta_4 - l_7}{l_5}\right) \quad \text{A-15}$$

$$s = l_4e^{1i\theta_4} + l_1e^{1i\theta_1} - l_5e^{1i\theta_5} \quad \text{A-16}$$

The angular velocities of the links are given in Equations A-17 through A-20 .

$$\omega_3 = \frac{l_2\omega_2}{(l_3\sin(\theta_4 - \theta_2))(\sin(\theta_3 - \theta_4))} \quad \text{A-17}$$

$$\omega_4 = \frac{l_2\omega_2}{(l_4\sin(\theta_2 - \theta_3))(\sin(\theta_4 - \theta_3))} \quad \text{A-18}$$

$$\omega_5 = \frac{l_4\omega_4}{l_5\cos\theta_4\cos\theta_5} \quad \text{A-19}$$

$$v_S = -l_4\omega_4 sin\theta_4 + l_5\omega_5 sin\theta_5 \quad \text{A-20}$$

The equations for the accelerations of the links are given in Equations

$$G = l_4 sin\theta_4 \quad \text{A-21}$$

$$H = l_3\sin\theta_3 \quad \text{A-22}$$

$$I = l_2\alpha_2 sin\theta_2 + l_2\omega_2^2 cos\theta_2 + \ l_3\omega_3^2 cos\theta_3 - l_4\omega_4^2 cos\theta_4 \quad \text{A-23}$$

$$J = l_4 cos\theta_4 \quad \text{A-24}$$

$$K = l_3 cos\theta_3 \quad \text{A-25}$$

$$L = l_2\alpha_2 cos\theta_2 - l_2\omega_2^2 cos\theta_2 + l_3\omega_3^2 cos\theta_3 - l_4\omega_4^2 cos\theta_4 \quad \text{A-26}$$

$$\alpha_3 = \frac{IJ - GL}{GK - HJ} \quad \text{A-27}$$

$$\alpha_4 = \frac{IK - HL}{GK - HJ} \quad \text{A-28}$$

$$M = l_4\alpha_4 cos\theta_4 - l_4\omega_4^2 sin\theta_4 + l_5\omega_5^2 sin\theta_5 \quad \text{A-29}$$

$$\alpha_5 = \frac{M}{l_5 cos\theta_5} \quad \text{A-30}$$

$$A_s = l_4\alpha_4 sin\theta_4 - l_4\omega_4^2 cos\theta_4 + l_5\alpha_5\sin\theta_5 + l_5\omega_5^2 cos\theta_5 \quad \text{A-31}$$

$$\boldsymbol{A}_b = l_2\alpha_2 e^{1i\left(\theta_2 + \frac{\pi}{2}\right)} - l_2\omega_2^2 e^{1i\theta_2} \quad \text{A-32}$$

$$\boldsymbol{A}_d = l_4\alpha_4 e^{1i\left(\theta_4 + \frac{\pi}{2}\right)} - l_4\omega_4^2 e^{1i\theta_4} \quad \text{A-33}$$

$$\boldsymbol{A}_{g3} = R_{23}\alpha_2 e^{1i\left(\theta_3+\frac{\pi}{2}\right)} - R_{23}\omega_3^2 e^{1i\theta_3} + \boldsymbol{A}_b \quad \text{A-34}$$

$$\boldsymbol{A}_{g4} = R_{14}\alpha_4 e^{1i\left(\theta_4+\frac{\pi}{2}\right)} - R_{14}\omega_4^2 e^{1i\theta_4} \quad \text{A-35}$$

$$\boldsymbol{A}_{g5} = R_{65}\alpha_5 e^{1i\left(\theta_5+\frac{\pi}{2}\right)} - R_{65}\omega_{45}^2 e^{1i\theta_5} + \boldsymbol{A}_d \quad \text{A-36}$$

Appendix B: Dynamic equilibrium system of equations

The following set of equations reference s Figure 2 and Figure 3. For these calculations, the input crank, link 2, is considered fully balanced. The set of dynamic equations for each link are now presented:

For Link 2

$$T_{12} - R_{32}cos\,\theta_2 F_{12y} + R_{32}sin\theta_2 F_{12x} = I_2\alpha_2 \quad \text{B-1}$$

Where I_2 is the moment of inertia of link 2.

For Link 3

$$F_{43x} - F_{32x} = m_3 A_{g3x} \quad \text{B-2}$$

$$F_{43y} - F_{32y} = m_3 A_{g3y} \quad \text{B-3}$$

$$\begin{aligned} R_{43}cos\theta_3 F_{43y} - R_{43}sin\theta_3 F_{43x} \\ - R_{23}sin\theta_3 F_{32x} \\ + R_{23}cos\theta_3 F_{32y} = I_3\alpha_3 \end{aligned} \quad \text{B-4}$$

For Link 4

$$\mathrm{F_{14x} + F_{54x} - F_{43x} = m_4 A_{g4x}} \quad \text{B-5}$$

$$\mathrm{F_{14y} + F_{54y} - F_{43y} = m_4 A_{g4y}} \quad \text{B-6}$$

$$\begin{aligned} -\mathrm{R_{14}sin\theta_4 F_{14y} + R_{14}cos\theta_4 F_{14x}} \\ + \mathrm{R_{54}cos\theta_4 F_{54y}} \\ - \mathrm{R_{54}sin\,\theta_4 F_{54x}} \\ + \mathrm{R_{34}sin\theta_4 F_{43x}} \\ - \mathrm{R_{34}cos\theta_4 F_{43y} = I_4\alpha_4} \end{aligned} \quad \text{B-7}$$

For Link 5

$$F_{65x} - F_{54x} = m_5 A_{g5x} \quad \text{B-8}$$

$$F_{65y} - F_{54y} = m_5 A_{g5y} \quad \text{B-9}$$

$$\begin{aligned} R_{65}cos\theta_5 F_{65y} - R_{65}sin\theta_5 F_{65x} \\ - R_{45}cos\theta_5 F_{54x} \\ + R_{45}sin\theta_5 F_{54y} \\ - R_{65}sin\theta_5 F_p = I_5\alpha_5 \end{aligned} \quad \text{B-10}$$

The slider provides 2 additional equations.

$$F_p - F_{65x} = m_s A_s \quad \text{B-11}$$

$$F_{16y} - F_{65y} = 0 \quad \text{B-12}$$

This system of equations can be solved for with a computer program or combined to find the solutions explicitly.